Theoretical Investigation of the Geometries and UV−vis Spectra of Poly(L-glutamic acid) Featuring a Photochromic Azobenzene Side Chain

Pierre-François Loos,*,[†] Julien Preat,[‡,§] Adèle D. Laurent,[‡] Catherine Michaux,[‡,⊥]
Denis Jacquemin,[‡,‖] Eric A. Perpète,[‡,‖,¶] and Xavier Assfeld[†]

*Equipe de Chimie et Biochimie Théoriques, UMR 7565 CNRS-UHP, Institut Jean
Barriol (FR CNRS 2843), Faculté des Sciences et Techniques, Nancy-Université, B.P.
239,54506 Vandoeuvre-les-Nancy Cedex, France, and Groupe de Chimie Physique
Théorique et Structurale, Facultés Universitaires Notre-Dame de la Paix, rue de
Bruxelles, 61, B-5000 Namur, Belgium*

Abstract: The geometries and UV−vis spectra of azobenzene dyes grafted as a side chain on poly(L-glutamic acid) have been investigated using a combination of quantum mechanics/molecular mechanics (QM/MM) and time-dependent density functional theory (TD-DFT) methods at the TD-PBE0/6-311+G(d,p)//B3LYP/6-311G(d,p):Amber ff99 level of theory. The influence of the secondary structure of the polypeptide on the electronic properties of both the trans and cis conformations of azobenzene dyes has been studied. It turns out that the grafted dyes exhibit a red-shift of the $\pi \rightarrow \pi^*$ absorption energies mainly due to the auxochromic shift induced by the peptidic group used to link the chromophoric unit to the polypeptide and that specific interactions between the glutamic side chain and the azobenzene moiety lead to a large blue-shift of the $n \rightarrow \pi^*$ transition.

1. Introduction

During the two last decades, the interest in azobenzene (AB) derivatives has become increasingly important due to their wide range of industrial applications. In particular, AB based molecules represent 60–70% of the world production of industrial "absorption" dyes[1] and have been recently found to be promising materials for media storage devices[2–5] and molecular motors.[6,7] These processes exploit the photochro-
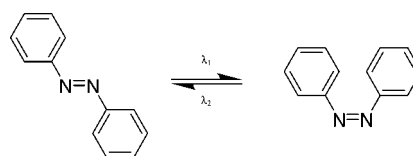
Figure 1. Reversible photochromic isomerization of the azobenzene derivative.

mic abilities of the AB dyes that are involved in a reversible photoisomerization from the trans (TAB) to the cis (CAB) isomer (Figure 1). In biological systems, the photoreversible isomerization of a molecule attached to a macromolecular system, such as the visual pigment rhodopsin,[8–14,39] induces conformational changes that in turn lead to a physiological response of the protein. Following this idea, Pieroni et al. have prepared poly(L-glutamic acid) with photochromic AB side chains[15–17] (Figure 2), that can exist in disordered forms (random coil) or in regularly folded structures (like α-helix or β-sheets), similar to biological systems. The photochromic polymers were prepared from high molecular weight poly(L-glutamic acid) ($\bar{M}_v$ = 200 000) and samples containing

* Corresponding author. E-mail: Pierre-Francois.Loos@cbt.uhp-nancy.fr.

† Nancy-Université.

‡ Facultés Universitaires Notre-Dame de la Paix.

§ Fellow of the Belgian Fund for the Formation to Research in Industry and Agriculture (FRIA).

⊥ Postdoctoral researcher of the Belgian National Fund for Scientific Research.

‖ Research associate of the Belgian National Fund for Scientific Research.

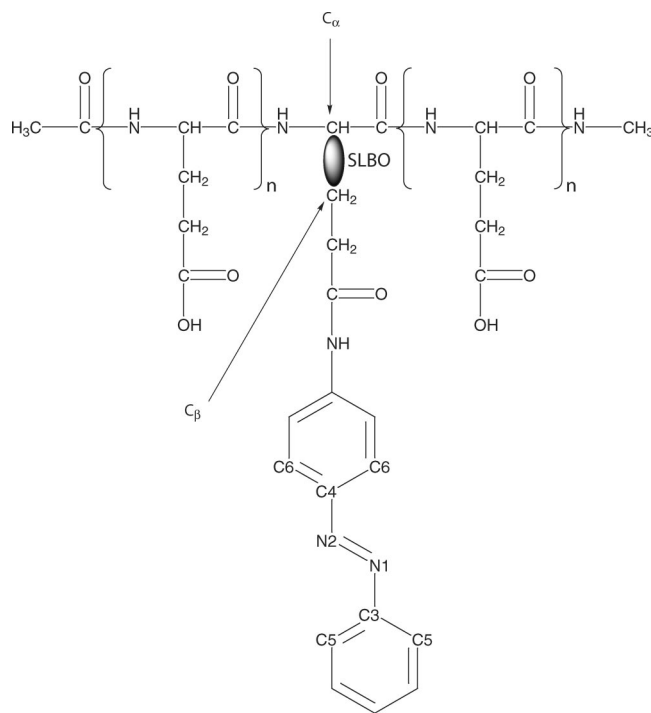¶ Invited professor at the Université Henri Poincaré (Nancy, France) from January to May 2007.

Figure 2. QM/MM partitioning of the poly(L-glutamic acid) with the photochromic AB side chain. The QM/MM boundaries are located between the C_α and the C_β atoms.

13–56% mol of azo groups were studied at different pH values. It has been shown that irradiation at 350 nm produces an isomerization from the trans to the cis isomer ($\pi \rightarrow \pi^*$ transition), whereas the reverse reaction is obtained using a 450 nm irradiation ($n \rightarrow \pi^*$ transition), or via dark adaptation.[15]

In water, this reversible process is accompagnied by large photoinduced structural changes of the polypeptide secondary structure, which is detected by circular dichroism (CD) spectroscopy, as well as a drastic modification of the absorption spectrum of the AB dye. Depending on the experimental conditions (pH and mole percent of azo group), the polypeptide presents a random coil, an α-helix, or a β-structure CD pattern with respect to the relative amount of each structure.[18] In acid pHs (4.7−5.0), the dark-adapted samples containing 16 and 21 mol % of azo groups indicate the presence of an appreciable amount of α-helix, while the 36 mol % samples exhibit the CD curve of β-structure. When the pH is increased to alkaline values (pH 8), all polypeptides undergo a conformational transition to random coil structures. In water, light produces the isomerization of the azo side chains and a remarkable effect on the CD bands, which is also influenced by the pH value and/or the azo content. For example, the 16 mol % sample does not exhibit any variation of the CD spectrum, while the 36 mol % azo-polypeptide undergoes a β-coil transition at pH 6.5. For the 21% azopolypeptide, the helix content is increased by irradiation below pH 6.3.

Prior to study the effect of experimental conditions (pH and azo content) and the dynamical behavior leading to the modification of the polypeptide conformation, this work aims at investigating the effects of the polypeptide structure on

the geometries and the absorption spectra of the two AB isomers (i.e., TAB and CAB).

From our point of view, to obtain accurate UV−vis spectra of macromolecular systems, one needs to take up two challenges:

• Due to the size of the system, the modeling of macromolecules with pure quantum mechanics is still out of reach for modern computational resources.

• To obtain accurate UV−vis spectra, one has to describe precisely the excited state(s) of the chromophoric unit.

Some propositions have been made to solve these challenges separately. For example, the size problem can be overcome with the hybrid quantum mechanics/molecular mechanics methods (QM/MM) which are available to treat such large systems.[19–29] For the second challenge, time-dependent density functional theory (TD-DFT) calculations[30] indeed yield accurate determination of the absorption energies associated with these excited states for a wide range of chromophoric units[31–36] and, especially, for the AB derivatives.[37,38,43]

One should note that only a limited number of studies combining QM/MM and TD-DFT methods have been previously published, such as the meticulous studies of Elstner et al.[13,14] and Vreven et al.,[39] who compare several computational approaches for the determination of the absorption shifts in retinal proteins. Rothlisberger and co-workers also report TD-DFT/MM calculations[40] on solvated acetone[41] and aminocoumarins[42] based on Car–Parrinello simulations. Altought Elstner et al. have shown that TD-DFT calculations fail dramatically in the case of protonated Schiff base chromophores and neutral polyenes[13,14] due to the local approximation of the exchange-correlation functional,[44] we would like to mention the successful work of Crecca and Roitberg on the isomerization mechanism of azobenzene and disubstitued azobenzene derivatives.[43] Using DFT and TD-DFT calculations, they have studied the isomerization pathway of several azobenzene derivatives. The different barriers of the potential energy surface have been found in good agreement with experimental results.

In this article, we report the calculation of UV−vis spectra of TAB and CAB units for various stable secondary and supersecondary structures (motifs) of the poly(L-glutamic acid). First, we investigate the geometries and the UV−vis spectra of both isomers in gas phase and in ethanol. The results are compared to experimental data to validate the theoretical scheme and to obtain some reference data in order to point out the specific effects of the polypeptide surroundings on the geometry and absorption wavelengths of the AB moiety. In particular, we investigate different polypeptide structures containing α-helix and β-sheet conformations, as well as other supersecondary structures like β-hairpin, β-strand, and β−α−β and α−β−α motifs.

2. Methodology

The QM/MM calculations are performed by means of the local self-consistent field (LSCF) method developed by Rivail, Assfeld, and co-workers,[47–56] that is implemented in a modified version of the Gaussian 03 package[57] linked to

Poly(L-glutamic acid) with AB Side Chain

J. Chem. Theory Comput., Vol. 4, No. 4, 2008 **639**

Table 1. Structures and UV−vis Spectra of TAB and CAB in Various Media, Obtained at the TD-PBE0/6-311+G(d,p)//B3LYP/6–311G(d,p) Level of Theory[a]

	medium	method	d(N=N)	d(C−N)	∠(C−N=N)	∠(C−C−N)	τ(C−C−N=N)	$\lambda^{n\to\pi*}$	$\lambda^{\pi\to\pi*}$	ref
TAB	gas phase	TD-DFT//DFT	1.253	1.418	115.1	124.6, 115.5	0.0, 180.0	480(0.00)	327(0.78)	37
		X-ray 1997 (82 K)	1.259	1.431	114.1		21.0			71
		GED 2001 (407 K)	1.260	1.428	113.7	124.8	0.0, 180.0			72
		exp 1981						444	303	73
		exp 1982						440(380)	301(21300)	69
	ethanol	TD-DFT//DFT	1.255	1.419	115.5	124.7, 115.5	0.0, 180.0	477(0.00)	344(0.90)	this work
		exp 1953						443(510)	320(21300)	74
		exp 1961						437(510)	320(17300)	75
CAB	gas phase	TD-DFT//DFT	1.243	1.436	124.1	122.9, 116.5	51.0, −138.1	478(0.03)	292(0.08)	this work
		X-ray 1971	1.253	1.449	121.9	122.5, 117.3	53.3			67
		exp 1982						425	265	69
	ethanol	TD-DFT//DFT	1.246	1.436	124.2	122.7, 116.5	50.8, −138.0	467(0.05)	305(0.09)	this work
		exp 1953						433(1518)	281(5260)	74
		exp 1973						443(1514)	281(5248)	76
TAB ⇌ CAB	gas phase	TD-DFT//DFT	−0.010	0.018	9.0	−1.7, 1.0	51.0, 41.9	−2	−35	this work
		X-ray	−0.006	0.018	7.8		32.3			67, 71
		exp						−19 → −15	−38 → −35	69, 73
	ethanol	TD-DFT//DFT	−0.009	0.017	8.7	−2.0, 1.0	50,8, 42.0	−10	−39	this work
		exp						−10 → +6	−39	74−76

[a] The changes in structural parameters and UV−vis spectra following to the reversible photoisomerization of both isomers are also reported. Distances are in angstroms, while the valence and the dihedral angles are in degrees. $\lambda^{n\to\pi*}$ and $\lambda^{\pi\to\pi*}$ are the wavelengths (in nanometers) of the first $n \to \pi*$ and $\pi \to \pi*$ transitions, respectively. The oscillator strengths are given in parenthesis.

the Tinker software[58] for the MM calculations. In the LSCF framework, a doubly occupied strictly localized bond orbital (SLBO) is employed to link the QM and the MM parts. The SLBO is obtained from a preliminary computation on a model molecule featuring the chemical bond of interest.[59] In the present case, the QM/MM frontier is located between the C_α and the C_β atoms of the residue where the azobenzene dye is grafted (Figure 2).

The MM surrounding is described with the Amber ff99 force field,[60,61] and we have considered the protonated form of the glutamic acid in order to avoid the spurious polarization due to negative charges on the glutamate anions. Then, we choose to mimic the effect of the counterions by the protonated state of the glutamic side chain. This strategy has been employed in several studies for biological systems[45,46] to mimic the situation in which the counterion is tightly bounded to the negatively charged moiety. The classical charge of the C_α frontier atom has been set to 0.0365 e instead of 0.0145 e to ensure the overall electroneutrality of the MM part. The van der Waals parameters for the QM atoms are set to the values defined for the corresponding atom type of the force field. Moreover, the N-terminus and C-terminus are capped with an acetyl and a *N*-methylamide group, respectively.

Concerning the QM calculations, the B3LYP functional[62] combined to the 6-311G(d,p) basis set has been used for geometry optimization of the chromophoric unit. After a full geometry optimization of the entire system, TD-DFT calculations have been performed to evaluate the UV−vis spectrum with the fitted-parameter-free PBE0 functional[63,64] and the 6-311+G(d,p) basis set. Previous studies have shown that, for the largest majority of organic dyes,[31–38] this theoretical scheme provides reliable results for geometrical parameters, as well as for the UV−vis spectra. To take into account solvent effects on the model systems, the polarizable continuum model (PCM) with UAKS atomic radii has been

used.[65] For TD-DFT calculations using SCRF solvation model, the nonequilibrium PCM method was selected.[66]

3. Results

3.1. TAB and CAB in the Gas Phase and in Ethanol. Table 1 reports the structural parameters and the UV−vis spectra of the TAB and CAB forms in the gas phase and in ethanol. As reported in a previous study,[37] direct comparisons of our results to experimental data might be impeded because X-ray structures are determined in the solid phase, whereas gas electron diffraction (GED) measurements are performed at relatively high temperature. Nevertheless, concerning the TAB isomer in the gas phase, B3LYP yields results with a maximal deviation of 0.013 Å for the bond lengths and 1.4° for the valence angles, if the most recent X-ray diffraction and GED experiments are used as references. Moreover, the GED measurements perfectly predict the planar gas-phase geometry of the TAB. For the CAB form, low-temperature X-ray experiments or GED measurements are not available in the literature, but the X-ray structure from ref 67 is in good agreement with our DFT results with a maximum deviation of 0.013 Å, 2.2°, and 2.3° for the bond lengths, valence, and dihedral angles, respectively.

Experimentally, the absorption UV−vis spectrum consists of low lying ($n \to \pi*$) bands between 380 and 520 nm which is a symmetry forbidden transition in the case of the trans isomer. The spectrum also exhibits a $\pi \to \pi*$ transition around 330 nm for TAB and 275 nm for CAB.[68]

For the UV−vis spectra of TAB, the TD-PBE0 absorption energies are in rather good agreement with the experimental values. Although the excitation energies are underestimated by 20–40 nm in gas phase or in ethanol, the hypsochromic/bathochromic shift for the $n \to \pi*/\pi \to \pi*$ are well-reproduced by the theoretical calculations. Experimentally, one notes a small shift between +3 and −7 nm for the $n \to$

π^* transition, to be compared to the -3 nm predicted by TD-PBE0 calculations. For the $\pi \rightarrow \pi^*$ excitation, we predict a bathochromic shift of $+17$ nm that is very close to the $+17$ and $+19$ nm experimentally obtained. We refer the reader to ref 37 for more details about the geometries and UV−vis transition of TAB.

Concerning the CAB absorption spectra, the deviation between theoretical and experimental results is of the same order of magnitude than those obtained for the trans isomer. The $n \rightarrow \pi^*$ excitation becomes a dipole-allowed transition due to the nonplanar geometry of the CAB derivative. Theoretically, taking into account the solvent effects, we observe an hypsochromic shift of -11 nm and a bathochromic shift of $+13$ nm for the $n \rightarrow \pi^*$ and $\pi \rightarrow \pi^*$ transitions, respectively. Compared to the TAB derivative, the solvent induces an increase of the hypsochromic shift for the $n \rightarrow \pi^*$ transition, while the $\pi \rightarrow \pi^*$ excitation energy remains unchanged with a clear decrease of the oscillator strength. The bathochromic effect of the solvent on the $\pi \rightarrow \pi^*$ excitation is well-reproduced by the present theoretical approach. Indeed, experimental results lead to a bathochromic shift of $+16$ nm. On the other hand, the red-shift of 8–18 nm, experimentally observed on the $n \rightarrow \pi^*$ transition, is not reproduced by TD-PBE0, which reports a blue-shift of -11 nm. However, the gas-phase UV−vis spectra of CAB is subject to caution: it is calculated at relatively high and variable temperature (181–322 °C) by means of a difference spectrum. This spectrum, obtained by a flash photolysis technique, corresponds to the difference between the absorption spectra of a stable compound (TAB), beforehand determined, and a metastable specie (CAB).[69]

Table 1 also reports the modification of the geometrical parameters and absorption wavelengths going with the photoisomerization of the AB dye (see Figure 1). The change of the C−N bond length is nicely reproduced, while the variations of the d(N=N) and $\angle$(C−N=N) values are slightly overestimated by the theoretical scheme. The largest discrepancy between theory and experiment comes from the overestimation of the variation of the τ(C−C−N=N) value by 10–20°, but these dihedral angle values might be very sensitive to the packing effect of the crystal. Nevertheless, the most recent GED experiment on the TAB gives a τ(C−C−N=N) value of 0.0°, that is a deviation between theory and experiment of 0.2° only. For the shift of the absorption wavelengths, the experimental and theoretical approaches predict blue-shift of the $n \rightarrow \pi^*$ and the $\pi \rightarrow \pi^*$ excitation energies in both the gas phase and ethanol. Moreover, TD-PBE0 provides energetic shifts in the range of the experimental figures, but for the shift of the $n \rightarrow \pi^*$ excitation in the gas phase. This observation blames once more the experimental $\lambda^{n \rightarrow \pi^*}$ value obtained in the case of CAB in the gas phase.

According to previous computational studies, the TD-DFT excitation energies are more red-shifted compared to other theoretical approaches like CC2 or SOPPA methods,[70] leading to a slightly larger discrepancy between the theoretical and experimental absolute wavelengths. However, this type of post Hartee−Fock methods are very time-consuming and, consequently, difficult to use for larger systems,

especially when solvent effects must be taken into account. In this case, DFT calculations using hybrid functionals such as B3LYP or PBE0 present a valuable accuracy/CPU balance. On top of that, these theoretical schemes have been proved reliable to reproduce the experimental shifts corresponding to solvatochromic effects and photoisomerization processes of the AB dye. We therefore apply this methodology in order to study the effect of the polypeptide structure on the absorption spectra of grafted AB moiety.

3.2. Poly(L-glumatic acid) with an AB Side Chain. Since the actual QM/MM method requires one SLBO to connect the QM to the MM part, it is important to check that it does not disturb the QM properties. The influence induced by the SLBO is analyzed in order to verify that no artificial shifts of the absorption energies in TD-DFT calculations are introduced. To do so, we computed the absorption wavelength of the QM part capped with a methyl group, at the QM level, with and without the SLBO (see Figure 2). On the basis of these preliminary calculations, one can conclude that the SLBO creates an error of 0.09 and 0.22 nm on the $n \rightarrow \pi^*$ and $\pi \rightarrow \pi^*$ transitions, respectively. Moreover, a previous study has demonstrated that the SLBO induces only slight modifications of the QM geometry.[59]

The geometrical parameters of the poly(L-glumatic acid) with AB side chain are listed in Table 2. We also report the optimized geometries and the number of glutamic residues corresponding to several secondary structures of the polypeptide (see Figure 3 for TAB and Figure 4 for CAB). Due to the importance of the N=N double bond length, the chromophoric unit of the AB dye, we first investigated its modifications. The various MM surroundings imply an increase of 0.002–0.004 Å, compared to the isolated TAB structure in the gas phase. Concerning the cis isomer of the poly(L-glumatic acid), the increase of the N=N distance is not systematic. Indeed, for the β-sheet, β-hairpin, and β-strand conformations of the MM part, the d(N1=N2) values are equal to or smaller (-0.001 Å) than the values of the isolated CAB structure. For the other secondary structures, the MM part induces an increase of the N=N bond length by 0.002–0.005 Å. The same effects are induced by the solvent (Table 1) for both isomers. The C−N distances are also affected by the polypeptide structure, as well as the angle values around the N=N chromophoric unit for both conformers. Contrary to the other geometrical parameters for which the effect of the MM surrounding is negligible, the dihedral angles are more affected by the polypeptide structure, leading to a nonplanar form of the TAB, regardless of the conformation of the MM part. For example, the α-helix conformation and the $\alpha-\beta-\alpha$ motif induce a τ(N1=N2−C4−C5) value of $\simeq 20°$. For the CAB derivatives, the α-containing structures (α-helix, $\alpha-\beta-\alpha$, and $\beta-\alpha-\beta$) lead to a large modification of the τ(N1=N2−C4−C6) values, yielding an increase of the N=N double bond as pointed above.

The UV−vis spectra of the poly(L-glumatic acid) containing AB side chain are reported in Table 3. For the TAB derivatives, an overall blue-shift (3–29 nm) and red-shift (23–36 nm) with respect to the isolated TAB molecule in the gas phase ($\Delta\lambda^{AB}$ values) are observed for

Poly(L-glutamic acid) with AB Side Chain

J. Chem. Theory Comput., Vol. 4, No. 4, 2008 **641**

Table 2. Structural Parameters of Isolated TAB and CAB and Grafted As Side Chain of Poly(L-glutamic acid) Obtained at the B3LYP/6-311G(d,p) Level of Theory[a]

MM structure	d (N1=N2)	d (C3—N1)	d (N2—C4)	∠(C3—N1=N2)	∠(N1=N2—C4)	∠(C5—C3—N1)	∠(N2—C4—C6)	τ(C5—C3—N1=N2)	τ(N1=N2—C4—C6)
TAB	1.253	1.418	1.418	115.1	115.1	124.6, 115.5	124.6, 115.5	0.0, 180.0	0.0, 180.0
α-helix	1.255	1.416	1.412	115.2	114.7	124.0, 116.1	124.4, 116.8	−23.5, 159.3	−12.2, 168.3
β−α−β	1.257	1.417	1.410	115.2	115.2	124.6, 115.6	124.7, 116.3	−7.8, 174.3	−3.2, −179.6
α−β−α	1.255	1.419	1.409	114.3	116.1	124.3, 116.0	125.9, 115.2	−8.0, 173.2	2.4, −175.6
β-sheet	1.255	1.417	1.412	115.1	115.3	124.7, 115.5	125.2, 115.9	−1.3, 178.5	−0.9, 178.1
β-hairpin	1.255	1.417	1.411	115.1	115.3	124.7, 115.6	125.1, 115.9	0.3, −179.7	0.2, −179.8
β-strand	1.255	1.415	1.415	115.1	115.7	124.3, 115.7	124.4, 116.4	17.2, −164.1	−18.3, 165.5
CAB	1.243	1.436	1.436	124.1	124.1	122.9, 116.5	122.9, 116.5	51.0, −138.1	51.0, −138.1
α-helix	1.245	1.433	1.430	124.4	125.1	122.0, 117.4	126.3, 114.6	−57.6, 131.4	−35.2, 154.0
β−α−β	1.248	1.428	1.427	125.7	127.9	122.5, 117.1	129.2, 112.5	−56.8, 133.0	−20.6, 166.6
α−β−α	1.246	1.431	1.429	125.5	126.2	121.2, 118.2	127.9, 113.5	65.2, −124.4	21.0, −166.9
β-sheet	1.242	1.441	1.434	123.2	123.5	119.8, 119.4	122.1, 118.1	73.5, −116.7	56.4, −133.9
β-hairpin	1.242	1.437	1.437	122.8	123.5	119.7, 119.4	121.3, 118.6	64.8, −125.6	58.8, −133.1
β-strand	1.243	1.431	1.436	123.5	125.0	122.9, 116.4	122.5, 117.4	51.9, −136.0	51.3, −139.4

[a] The MM part is described with the Amber ff99 force field. Distances are in angstroms, while the valence and the dihedral angles are in degrees. See Figure 2 for the atom labeling.
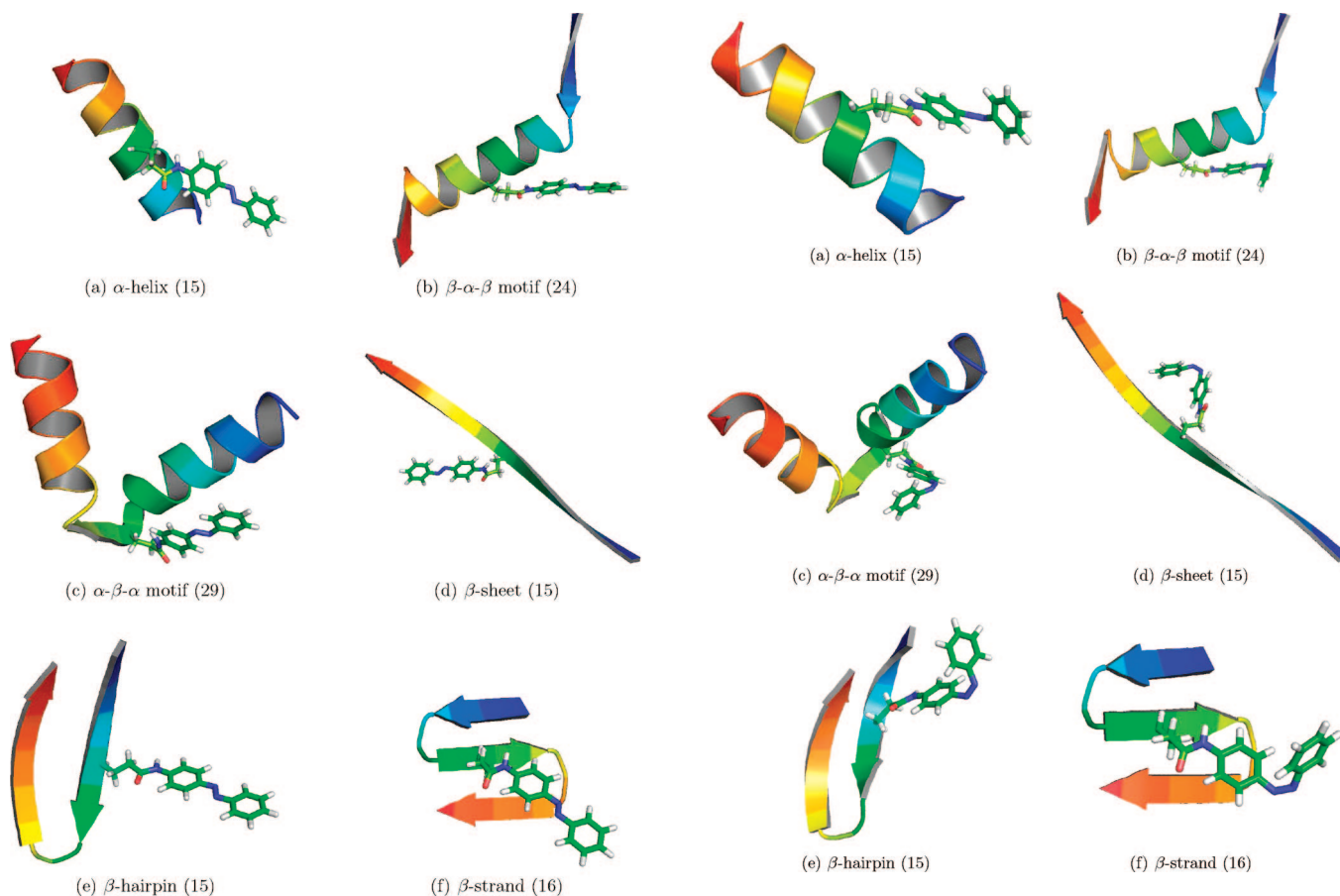
Figure 3. QM/MM optimized geometries of the poly(L-glutamic acid) with the photochromic TAB side chain. The QM part is depicted as a stick model, while the MM structure has a cartoon representation. We also report the number of glutamic residues in parenthesis.

(a) α-helix (15)
(b) β-α-β motif (24)
(c) α-β-α motif (29)
(d) β-sheet (15)
(e) β-hairpin (15)
(f) β-strand (16)

Figure 4. QM/MM optimized geometries of the Poly(L-glutamic acid) with the photochromic CAB side chain. The QM part is depicted as a stick model, while the MM structure has a cartoon representation. We also report the number of glutamic residues in parenthesis.

(a) α-helix (15)
(b) β-α-β motif (24)
(c) α-β-α motif (29)
(d) β-sheet (15)
(e) β-hairpin (15)
(f) β-strand (16)

the $n \rightarrow \pi^*$ and $\pi \rightarrow \pi^*$ transitions, respectively. This is in full agreement with previous results on substituted TAB derivatives.[38] It is noteworthy that the $n \rightarrow \pi^*$ transition in TAB is no more symmetry-forbidden and significant, though small oscillator strengths are observed, especially for the α-helix conformation and the $\beta-\alpha-\beta$ motif. The

overall red-shift of the $\pi \rightarrow \pi^*$ band is also observed in the case of the CAB derivatives (21–32 nm), notwithstanding that the blue-shift of the $n \rightarrow \pi^*$ is not systematic: the conformations mainly featuring β structures (β-sheet, β-hairpin, and β-strand) show a blue-shift of −20, −15, and −21 nm, respectively, whereas the α-containing structures lead to a red-shift of 10–14 nm.

Table 3. UV−vis Spectra of the TAB and CAB Grafted on the Side Chain of Poly(L-glutamic acid) Obtained at the TDPBE0/6-311+G(d,p) Level of Theory[a]

| | MM structure | $\lambda^{n\rightarrow\pi^*}$ | $\Delta\lambda^{AB}$ | | | | $\lambda^{\pi\rightarrow\pi^*}$ | $\Delta\lambda^{AB}$ | | | | $\Delta\lambda^{max}$ |
			tot	$\Delta\lambda^{elec}$	$\Delta\lambda^{nuc}$	$\Delta\lambda^{aux}$		tot	$\Delta\lambda^{elec}$	$\Delta\lambda^{nuc}$	$\Delta\lambda^{aux}$	
TAB	α-helix	469(0.04)	−11	0	−7	−4	350(0.94)	23	0	−7	30	119
	β−α−β	477(0.01)	−3	0	1	−4	363(1.00)	36	3	3	30	114
	α−β−α	475(0.00)	−5	1	−2	−4	361(1.02)	34	2	2	30	114
	β-sheet	477(0.00)	−3	0	1	−4	357(0.98)	30	2	−2	30	120
	β-hairpin	476(0.00)	−4	1	−1	−4	359(0.87)	32	0	2	30	117
	β-strand	451(0.00)	−29	−21	−4	−4	358(0.75)	31	5	−4	30	93
CAB	α-helix	488(0.05)	10	−1	2	9	314(0.35)	22	−1	0	23	174
	β−α−β	492(0.06)	14	−16	21	9	324(0.47)	32	5	4	23	168
	α−β−α	492(0.04)	14	−2	7	9	316(0.50)	24	3	4	23	176
	β-sheet	458(0.04)	−20	0	−29	9	315(0.12)	23	1	−1	23	143
	β-hairpin	463(0.05)	−15	0	−24	9	313(0.15)	21	−6	4	23	150
	β-strand	457(0.08)	−21	−25	−5	9	323(0.18)	31	4	4	23	134

[a] The MM part is described with the help of the Amber ff99 force field. $\lambda^{n\rightarrow\pi^*}$ and $\lambda^{\pi\rightarrow\pi^*}$ are the wavelengths (in nanometers) of the first $n \rightarrow \pi^*$ and $\pi \rightarrow \pi^*$ transitions, respectively. The oscillator strengths are given in parenthesis. We also report the energetic shift (in nanometers) between the TD-DFT/MM values and the AB in gas phase ($\Delta\lambda^{AB}$). The $\Delta\lambda^{AB}$ value is decomposed in three components coming from the electronic polarization of the MM charges ($\Delta\lambda^{elec}$), the nuclear polarization of the MM surrounding ($\Delta\lambda^{nuc}$), and the auxochromic shift due to the substitution of the AB moiety ($\Delta\lambda^{aux}$), such as $\Delta\lambda^{AB} = \Delta\lambda^{elec} + \Delta\lambda^{nuc} + \Delta\lambda^{aux}$.
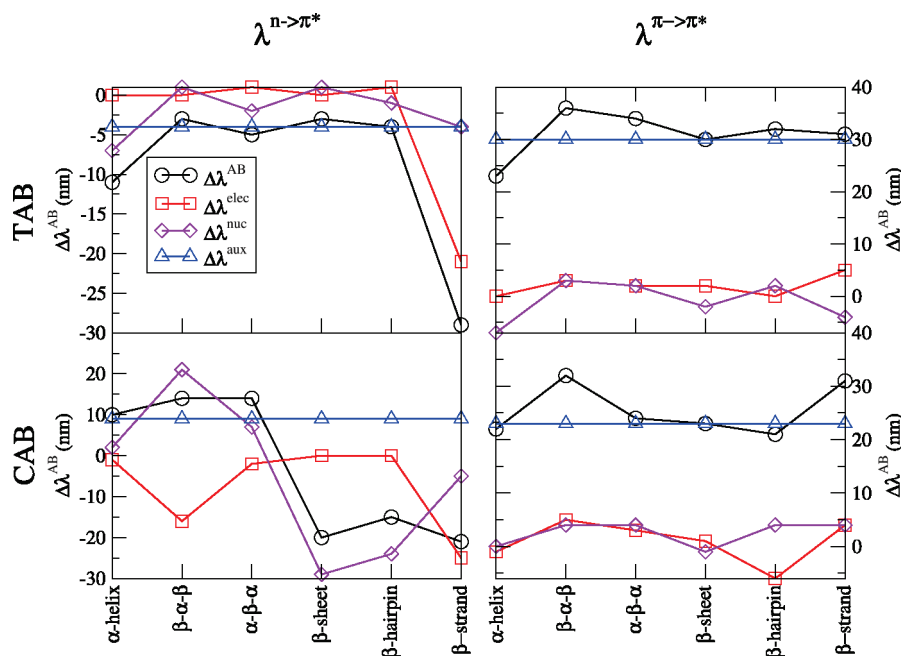

Figure 5. Energetic shift (in nanometers) between the TD-DFT/MM values and the AB in the gas phase ($\Delta\lambda^{AB}$). The $\Delta\lambda^{AB}$ value is decomposed in three components coming from the electronic polarization of the MM charges ($\Delta\lambda^{elec}$), the nuclear polarization of the MM surrounding ($\Delta\lambda^{nuc}$), and the auxochromic shift due to the substitution of the AB moiety ($\Delta\lambda^{aux}$), such as $\Delta\lambda^{AB} = \Delta\lambda^{elec} + \Delta\lambda^{nuc} + \Delta\lambda^{aux}$.

In order to better understand the physical meaning of these results, the $\Delta\lambda^{AB}$ values are split up in three components gathered in Table 3 and depicted in Figure 5:

• The polarization of the electronic wave function due to the MM classical point charges of the force field ($\Delta\lambda^{elec}$). These quantities are determined by the difference between the TD-DFT/MM calculations obtained with electronic embedding (EE) and the results of the TD-DFT/MM calculations in which the point charges are set to zero with the same geometry.

• The geometrical modification of the QM part geometries with respect to the capped primary system (CPS) induced by the MM surroundings ($\Delta\lambda^{nuc}$). The CPS corresponds to the QM part capped with an hydrogen atom (Figure 2). These energetic shifts are obtained by the difference between the TD-DFT/MM results with the MM point charges set to zero and the TD-DFT values on the optimized structures of the CPS. This effect corresponds to the polarization of the MM surrounding on the nuclei positions.

• $\Delta\lambda^{aux}$ which corresponds to the shift implied by the auxochromic groups (including the amide group and an alkyl chain) used to graft the photochromic AB to the polypeptide backbone. This quantity, independent of the polypeptide conformation, is defined as the difference of the excitation energies between the CPS and the AB moiety.

According to these definitions, the overall shift of the absorption energy when going from the isolated AB mol-

ecules to the full system is defined by: $\Delta\lambda^{AB} = \Delta\lambda^{elec} + \Delta\lambda^{nuc} + \Delta\lambda^{aux}$.

For the $\pi \rightarrow \pi*$ transitions in the TAB derivatives, the main component of the red-shift comes from the auxochromic contribution $\Delta\lambda^{aux}$. Indeed, the polarization due to the MM environment on the electronic wave function and the nuclei positions leads to only small modifications of the $\lambda^{\pi \rightarrow \pi*}$ values. However, further investigations of the $\Delta\lambda^{elec}$ values show that the polarization of the MM point charges also implies a red-shift of 0–5 nm. For the $n \rightarrow \pi*$ excitation, the situation is slightly different with a much smaller auxochromic effect (blue-shift of −4 nm). We point out the effect of the EE which implies a large blue-shift (−21 nm) in the case of the β-hairpin structure. This effect corresponds to a stabilization of the ground-state compared to the excited state and originates from a specific interaction of the carboxylic acid hydrogen atom of the glutamic acid side chain with the lone pair of the N=N chromophoric unit of the TAB moiety (see Figure 6). This highligths the key role that can be played by the glumatic acid side chain of the polypeptide. Similar to the specific solvent–solute interactions, the intramolecular interaction between the chromophoric unit and the polypeptide may induce a strong shift of the excitation energies and especially for the $n \rightarrow \pi*$ transition. Indeed, these two orbitals correspond to a localized phenomenon: the n nonbonding (Figure 6a) and the $\pi*$ antibonding (Figure 6c) orbitals are mainly localized on the chromophoric units of the AB dye. The n orbital corresponds to the nitrogen lone pair, while the $\pi*$ orbital is mainly located on the diazo bond. The $\lambda^{\pi \rightarrow \pi*}$ value is less affected by these specific interactions ($\Delta\lambda^{elec} = +5$ nm) due to the nature of the π bonding orbital, which is delocalized over the whole molecule (Figure 6b).

The investigation of the $\pi \rightarrow \pi*$ excitations in the CAB derivatives leads to conclusions similar to the case of the trans isomers. The red-shift of the absorption energies is mainly due to the substitution effect on the AB moiety. For the $n \rightarrow \pi*$ transition, the β-containing structure exhibit a blue-shift of the excitation wavelengths. The β-strand case is explained by the same phenomenon than for the TAB derivatives, whereas the results of the β-sheet and β-strand conformations shows a clear dependence upon the modification of the AB geometries, as illustrated by the $\Delta\lambda^{nuc}$ values. As previously mentionned, both β-sheet and β-strand conformations exhibit the smallest N=N bond length and the largest $d(C-N)$ values (Table 2). The effect, albeit less pronounced, is still present in the β-strand structure, whereas the opposite phenomenon is observed for the $\beta-\alpha-\beta$ motif. The increase of the N=N chromophoric unit leads to a $\Delta\lambda^{nuc}$ value of +21 nm. However, this MM conformation does not induce a large red-shift of the absorption energies due to a balanced effect with the $\Delta\lambda^{elec}$ value, as a consequence of the proximity of a glutamic side chain to the AB moiety.

4. Conclusions

On the basis of a theoretical approach combining QM/MM and TD-DFT calculations, we have reported the obtention of the UV−vis spectra of poly(L-glutamic) acid modified with chromophoric AB side chain at the TD-PBE0/6-311+G(d,p)//
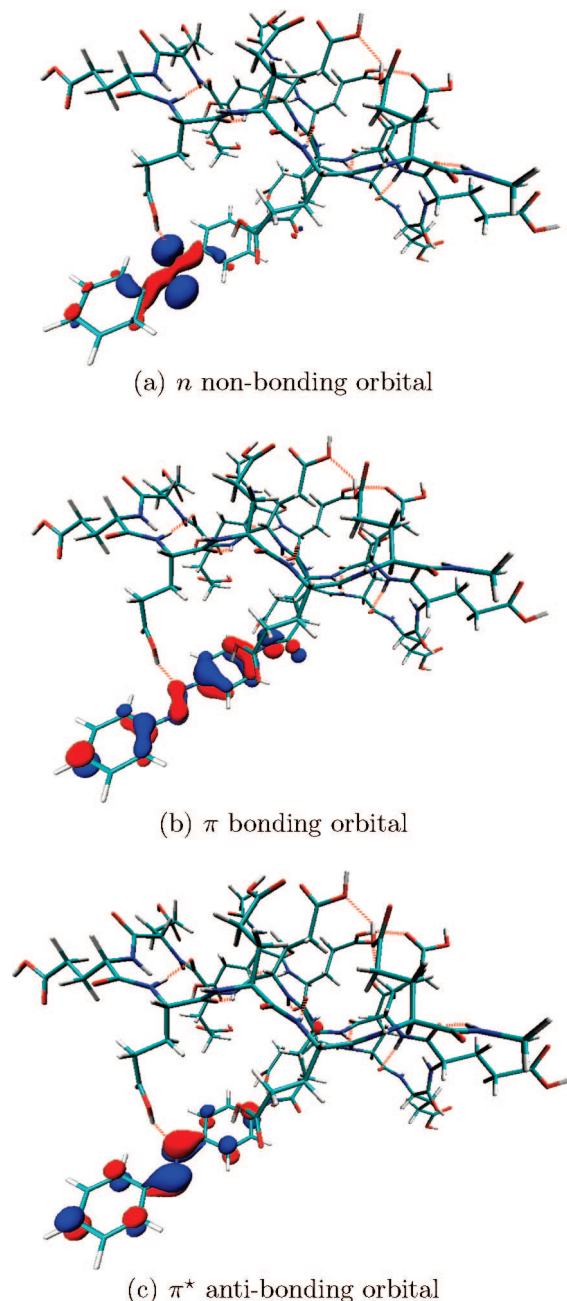

(a) n non-bonding orbital

(b) π bonding orbital

(c) π^* anti-bonding orbital

Figure 6. Isosurface (0.05 au$^{-3/2}$) of the frontier orbitals involved in the $n \rightarrow \pi^*$ and $\pi \rightarrow \pi^*$ transitions of the TAB grafted on a polypeptide with a β-strand conformation.

B3LYP/6-311G(d,p) level of theory using the Amber ff99 force field to treat the MM part. The results on the AB units, in both the gas phase and in ethanol, indicate that this theoretical approach is able to provide geometries and absorption wavelengths that are in good agreement with the available experimental data. In particular, we have shown that the TD-PBE0 results reproduce the energetic shifts due to the solvatochromic effects and the photoisomerization process of the AB dye.

In order to foresee the effect of the polypeptide structure, we have studied the polarization effect on the UV−vis spectra of the AB derivatives of several stable conformations featuring regularly folded structures, such as α-helix and β-sheet, on the UV−vis spectra of the AB derivatives. It

has been shown that the $\pi \rightarrow \pi^*$ absorption energies are globally red-shifted. This effect has been ascribed to a large auxochromic shift mainly due to the amide group used to graft the AB moiety to the carboxylic group of the glutamic side chain. Moreover, specific interactions between the glutamic side chain and the azobenzene moiety, such as hydrogen bond or large geometrical changes of the QM part, may lead to a large blue-shift on the $n \rightarrow \pi^*$ transition.

We are currently investigating the dynamic behavior of the AB photoisomerization in the framework of multiscale QM/MM dynamics in order to point out the major phenomena that could lead to strong modifications of the polypeptide secondary structure.

References

(1) Zollinger, H. In *Color Chemisrty, Syntheses, Properties and Applications of Organic Dyes and Pigments*, 3rd ed.; Wiley-VCH: Weinheim, 2003.

(2) Sudesh Kumar, G.; Neckers, D. C. *Chem. Rev.* **1989**, *89*, 1915–1925.

(3) Tamai, N.; Miyasaka, H. *Chem. Rev.* **2000**, *100*, 1875–1890.

(4) Natansohn, A.; Rochon, P. *Chem. Rev.* **2002**, *102*, 4139–4176.

(5) Yu, Y.; Nakano, M.; Ikeda, T. *Nature* **2003**, *425*, 145.

(6) Balzani, V.; Credi, A.; Raymo, F. M.; Stoddart, J. F. *Angew. Chem., Int. Ed.* **2000**, *39*, 3348–3391.

(7) Qu, C. J.; Wang, Q. C.; Ren, J.; Tian, H. *Org. Lett.* **2004**, *6*, 2085–2088.

(8) Mathies, R. A.; Lugtenburg, J. In *Handbook of Biological Physics*; Stavenga, D. G., de Grip, W. J., Pugh, E. N., Eds.; Elsevier Science B. V.: New York, 2000; Vol. 3.

(9) Ferré, N.; Olivucci, M. *J. Am. Chem. Soc.* **2003**, *125*, 6868–6869.

(10) Andruniow, T.; Ferré, N.; Olivucci, M. *Proc. Natl. Acad. Sci. USA* **2004**, *101*, 17908–17913.

(11) Coto, P. B.; Sinicropi, A.; Ferré, N.; Olivucci, M. *Proc. Natl. Acad. Sci. USA* **2006**, *103*, 17154–17159.

(12) Frutos, L. M.; Andruniow, T.; Santoro, F.; Ferré, N.; Olivucci, M. *Proc. Natl. Acad. Sci. USA* **2007**, *104*, 7764–7769.

(13) Wanko, M.; Garavelli, M.; Bernardi, F.; Niehaus, T. A.; Frauenheim, T.; Elstner, M. *J. Chem. Phys.* **2004**, *120*, 1674–1692.

(14) Wanko, M.; Hoffmann, M.; Strodel, P.; Koslowski, A.; Thiel, W.; Neese, F.; Frauenheim, T.; Elstner, M. *J. Phys. Chem. B* **2005**, *109*, 3606–3615.

(15) Pieroni, O.; Houben, J. L.; Fissi, A.; Constantino, P.; Ciardelli, F. *J. Am. Chem. Soc.* **1980**, *102*, 5913–5915.

(16) Houben, J. L.; Fissi, A.; Bacciola, D.; Rosato, N.; Pieroni, O.; Ciardelli, F. *Int. J. Biol. Macromol.* **1983**, *5*, 94–100.

(17) Ciardelli, F.; Pieroni, O.; Fissi, A.; Houben, J. L. *Biopolymers* **1984**, *23*, 1423–1437.

(18) Pieroni, O.; Fissi, A.; Angelini, N.; Lenci, F. *Acc. Chem. Res.* **2001**, *34*, 9–17.

(19) Warshell, A.; Levitt, M. *J. Mol. Biol.* **1976**, *103*, 227–249.

(20) Singh, U. C.; Kollman, P. A. *J. Comput. Chem.* **1986**, *7*, 718–730.

(21) Field, M. J.; Bash, P. A.; Karplus, M. *J. Comput. Chem.* **1990**, *11*, 700–733.

(22) Das, D.; Eurenius, K. P.; Billings, E. M.; Sherwood, P.; Chatfield, D. C.; Hodoseek, M.; Brooks, B. R. *J. Chem. Phys.* **2002**, *117*, 10534–10547.

(23) Zhang, Y.; Lee, T.-S.; Yang, W. *J. Chem. Phys.* **1999**, *110*, 46–54.

(24) Antes, I.; Thiel, W. *J. Phys. Chem. A* **1999**, *103*, 9290–9295.

(25) DiLabio, G. A.; Hurley, M. M.; Christiansen, P. A. *J. Chem. Phys.* **2002**, *166*, 9578–9584.

(26) Philipp, D. M.; Friesner, R. A. *J. Comput. Chem.* **1999**, *20*, 1468–1494.

(27) Pu, J.; Gao, J.; Truhlar, D. G. *J. Phys. Chem. A* **2004**, *108*, 632–650.

(28) Kairys, V.; Jensen, J. H. *J. Phys. Chem. A* **2000**, *104*, 6656–6665.

(29) Lin, H.; Truhlar, D. G. *J. Phys. Chem. A* **2005**, *109*, 3991–4004.

(30) Runge, E.; Gross, E. K. U. *Phys. Rev. Lett.* **1984**, *52*, 997–1000.

(31) Preat, J.; Jacquemin, D.; Perpete, E. A. *Chem. Phys. Lett.* **2005**, *415*, 20–24.

(32) Preat, J.; Jacquemin, D.; Wathelet, V.; André, J.-M.; Perpete, E. A. *J. Phys. Chem. A* **2006**, *110*, 8144–8150.

(33) Jacquemin, D.; Preat, J.; Wathelet, V.; Fontaine, M.; Perpete, E. A. *J. Am. Chem. Soc.* **2006**, *128*, 2072–2083.

(34) Preat, J.; Loos, P.-F.; Assfeld, X.; Jacquemin, D.; Perpete, E. A. *Int. J. Quantum Chem.* **2007**, *107*, 574–585.

(35) Preat, J.; Loos, P.-F.; Assfeld, X.; Jacquemin, D.; Perpete, E. A. *J. Mol. Struct. (THEOCHEM)* **2007**, *808*, 85–91.

(36) Preat, J.; Jacquemin, D.; Wathelet, V.; André, J.-M.; Perpete, E. A. *Chem. Phys.* **2007**, *335*, 177–186.

Poly(L-glutamic acid) with AB Side Chain

J. Chem. Theory Comput., Vol. 4, No. 4, 2008 **645**

(37) Briquet, L.; Vercauteren, D. P.; Perpete, E. A.; Jacquemin, D. *Chem. Phys. Lett.* **2006**, *417*, 190–195.

(38) Briquet, L.; Vercauteren, D. P.; André, J.-M.; Perpete, E. A.; Jacquemin, D. *Chem. Phys. Lett.* **2007**, *435*, 257–262.

(39) Vreven, T.; K.; Morokuma, K. *Theor. Chem. Acc.* **2003**, *109*, 125–132.

(40) Moret, M.-E.; Tapavicza, E.; Guidoni, L.; Rohrig, U. F.; Sulpizi, M.; Tavernelli, I.; Rothlisberger, U. *Chimia* **2005**, *59*, 493–498.

(41) Roehrig, U. F.; Frank, I.; Hutter, J.; Laio, A.; VandeVondele, J.; Rothlisberger, U. *Chem. Phys. Chem* **2003**, *4*, 1177–1182.

(42) Sulpizi, M.; Carloni, P.; Hutter, J.; Rothlisberger, U. *Phys. Chem. Chem. Phys.* **2003**, *5*, 4798–4805.

(43) Crecca, C. R.; Roitberg, A. E. *J. Phys. Chem. A* **2006**, *110*, 8188–8203.

(44) Dreuw, A.; Head-Gordon, M. *Chem. Rev.* **2005**, *105*, 4009–4037.

(45) Gu, J.; Xie, Y.; Schaefer, H. F., III *J. Am. Chem. Soc.* **2005**, *127*, 1053–1057.

(46) Gu, J.; Xie, Y.; Schaefer, H. F., III *J. Am. Chem. Soc.* **2005**, *127*, 1250–1252.

(47) Assfeld, X.; Rivail, J.-L. *Chem. Phys. Lett.* **1996**, *263*, 100–106.

(48) Ferré, N.; Assfeld, X.; Rivail, J.-L. *J. Comput. Chem.* **2002**, *23*, 610–624.

(49) Ferré, N.; Assfeld, X. *J. Chem. Phys.* **2002**, *117*, 4119–4125.

(50) Ferré, N.; Assfeld, X. *J. Mol. Struct. (Theochem)* **2003**, *632*, 83–90.

(51) Moreau, Y.; Loos, P.-F.; Assfeld, X. *Theor. Chem. Acc.* **2004**, *112*, 228–239.

(52) Moreau, Y.; Assfeld, X. *Lecture Ser. Comput. Comput. Sci.* **2005**, *3*, 1–9.

(53) Fornili, A.; Loos, P.-F.; Sironi, M.; Assfeld, X. *Chem. Phys. Lett.* **2006**, *427*, 236–240.

(54) Loos, P.-F.; Assfeld, X. *J. Chem. Theory Comput.* **2007**, *3*, 1047–1053.

(55) Loos, P.-F.; Assfeld, X. *Int. J. Quantum Chem.* **2007**, *107*, 2243–2252.

(56) Loos, P.-F.; Assfeld, X. *AIP Conf. Proc.* **2007**, *963*, 308–315.

(57) Frisch, M. J.; Trucks, G. W.; Schlegel, H. B.; Scuseria, G. E.; Robb, M. A.; Cheeseman, J. R.; Montgomery, J. A., Jr.; Vreven, T.; Kudin, K. N.; Burant, J. C.; Millam, J. M.; Iyengar, S. S.; Tomasi, J.; Barone, V.; Mennucci, B.; Cossi, M.; Scalmani, G.; Rega, N.; Petersson, G. A.; Nakatsuji, H.; Hada, M.; Ehara, M.; Toyota, K.; Fukuda, R.; Hasegawa, J.; Ishida, M.; Nakajima, T.; Honda, Y.; Kitao, O.; Nakai, H.; Klene, M.; Li, X.; Knox, J. E.; Hratchian, H. P.; Cross, J. B.; Bakken, V.; Adamo, C.; Jaramillo, J.; Gomperts, R.; Strat-mann, R. E.; Yazyev, O. ; Austin, A. J.; Cammi, R.; Pomelli, C.; Ochterski, J. W.; Ayala, P. Y.; Morokuma, K.; Voth, G. A.; Salvador, P.; Dannenberg, J. J.; Zakrzewski, V. G.; Dapprich, S.; Daniels, A. D.; Strain, M. C.; Farkas, O.; Malick, D. K.; Rabuck, A. D.; Raghavachari, K.; Foresman, J. B.; Ortiz, J. V.; Cui, Q.; Baboul, A. G.; Clifford, S.; Cioslowski, J. ; Stefanov, B. B.; Liu, G.; Liashenko, A.; Piskorz, P.; Komaromi, I.; Martin, R. L.; Fox, D. J.; Keith, T.; Al-Laham, M. A.; Peng, C. Y.; Nanayakkara, A.; Challacombe, M.; Gill, P. M. W.; Johnson, B.; Chen, W.; Wong, M. W.; Gonzalez, C.; Pople, J. A. *Gaussian 03*, revision 0.05; Gaussian, Inc.: Wallingford, CT,2004.

(58) Ponder, J. W. *Tinker*, version 4.2; Washington University: St. Louis, MO, 2004.

(59) Fornili, A.; Moreau, Y.; Sironi, M.; Assfeld, X. *J. Comput. Chem.* **2006**, *27*, 515–523.

(60) Cornell, W. D.; Cieplak, P.; Bayly, C. I.; Gould, I. R.; Merz, K. M., Jr.; Ferguson, D. M.; Spellmeyer, D. C.; Fox, T.; Caldwell, J. W.; Kollman, P. A. *J. Am. Chem. Soc.* **1995**, *117*, 5179–5197.

(61) Wang, J.; Cieplak, P.; Kollman, P. A. *J. Comput. Chem.* **2000**, *21*, 1049–1074.

(62) Becke, A. D. *J. Chem. Phys.* **1993**, *98*, 5648–5652.

(63) Ernzerhof, M.; Scuseria, G. E. *J. Chem. Phys.* **1999**, *110*, 5029–5036.

(64) Adamo, C.; Barone, V. *J. Chem. Phys.* **1999**, *110*, 6158–6170.

(65) Tomasi, J.; Mennucci, B.; Cammi, R. *Chem. Rev.* **2005**, *105*, 2999–3094.

(66) Cossi, M.; Barone, V. *J. Chem. Phys.* **2001**, *115*, 4708–4717.

(67) Mostad, A.; Romming, C. *Acta Chem. Scand.* **1971**, *25*, 3561–3568.

(68) Nagele, T.; Hoche, R.; Zinth, W.; Wachtveitl, J. *Chem. Phys. Lett.* **1997**, *272*, 489–495.

(69) Andersson, J.-A.; Petterson, R.; Tegner, L. *J. Photochem.* **1982**, *20*, 17–32.

(70) Fliegl, H.; Kohn, A.; Hattig, C.; Ahlrichs, R. *J. Am. Chem. Soc.* **2003**, *125*, 9812–9827.

(71) Harada, J.; Ogawa, K.; Tomoda, S. *Acta Cryst. B* **1997**, *53*, 662–672.

(72) Tsuji, T.; Takashima, H.; Takeuchi, H.; Egawa, T.; Konaka, S. *J. Phys. Chem. A* **2001**, *105*, 9347–9353.

(73) Millefiori, S.; Millefiori, A. *J. Chem. Soc., Faraday Trans. II* **1981**, *77*, 245–258.

(74) Birnhaum, P. P.; Linford, J. H.; Style, D. W. G. *Trans. Faraday Soc.* **1953**, *49*, 735–744.

(75) Gore, P. H.; Wheeler, O. H. *J. Org. Chem.* **1961**, *26*, 3295–3298.

(76) Grasselli, J. G. In *CRC Atlas of Spectral Data and Physical Constants for Organic Compounds*; CRC Press: Cleveland, OH, 1973.